

On the newtonian limit and cut–off scales of isothermal dark matter halos with cosmological constant.

Roberto A. Sussman¹ and Xavier Hernandez²

¹ *Instituto de Ciencias Nucleares, Universidad Nacional Autónoma de México A. P. 70–543, México 04510 D.F., México.*

² *Instituto de Astronomía, Universidad Nacional Autónoma de México A. P. 70–264, México 04510 D.F., México*

29 October 2018

ABSTRACT

We examine isothermal dark matter halos in hydrostatic equilibrium with a “ Λ -field”, or cosmological constant $\Lambda = \Omega_\Lambda \rho_{\text{crit}} c^2$, where $\Omega_\Lambda \simeq 0.7$, and ρ_{crit} is the present value of the critical density with $h \simeq 0.65$. Modeling cold dark matter as a self-gravitating Maxwell-Boltzmann gas, the Newtonian limit of General Relativity yields equilibrium equations that are different from those arising by merely coupling an “isothermal sphere” to the Λ -field within a Newtonian framework. Using the conditions for the existence and stability of circular geodesic orbits, the numerical solutions of the equilibrium equations (Newtonian and Newtonian limit) show the existence of (I) an “isothermal region” ($0 \leq r < r_2$), where circular orbits are stable and all variables behave almost identically to those of an isothermal sphere; (II) an “asymptotic region” ($r > r_1$) dominated by the Λ -field, where the Newtonian potential oscillates and circular orbits only exist in disconnected patches of the domain of r ; (III) a “transition region” ($r_2 \leq r < r_1$) between (I) and (II), where circular orbits exist but are unstable. We also find that no stable configuration can exist with central density, ρ_c , smaller than 2Λ , hence any galactic haloes which virialized at $z < 30$ in a Λ -CDM cosmological background must have central densities of $\rho_c > 0.008 M_\odot/\text{pc}^3$, in interesting agreement with rotation curve studies of dwarf galaxies. Since r_2 marks the largest radius of a stable circular orbit, it provides a characteristic boundary or “cut off” maximal radius for isothermal spheres in equilibrium with a Λ -field. For current estimates of ρ_c and velocity dispersion of virialized galactic structures, this cut off scale ranges from 90 kpc for dwarf galaxies, up to to 3 Mpc for large galaxies and 22 Mpc for clusters. In a purely Newtonian framework these length scales are about 10% smaller, though in either case r_2 is between five and seven times larger than physical cut off scales of isothermal halos, such as the virialization radius or the critical radius for the onset of Antonov instability. These results indicate that the effects of the Λ -field can be safely ignored in studies of virialized structures, but could be significant in the study of structure formation models and the dynamics of superclusters still in the linear regime or of gravitational clustering at large scales ($r \approx 30$ Mpc).

Key words: gravitation – relativity – galaxies: haloes – galaxies: formation – cosmology: theory

1 INTRODUCTION

Recent observational data from type Ia supernovae and CMB anisotropies suggests that large scale cosmic dynamics are dominated by a repulsive type of matter–energy density, generically known as a “dark energy”. In its most simple empirical formulation, dark energy can be described as a “ Λ -field” associated with the “cosmological constant”. More sophisticated models of dark energy take the form of scalar

field sources in which the Λ -field corresponds to the limit of vanishing scalar field gradients. This paper addresses an important issue in this context, namely: to examine if this type of repulsive interaction has any influence on the equilibrium of virialized galactic halo structures. Various aspects regarding this question have been considered previously in the literature. Lahav et al. (1991) have argued, using Newtonian spherical infall models (or “top hat” models), that the effects of a cosmological constant can be neglected in the

study of structure formation. Further improvements of “top hat” models incorporating Λ and/or quintessence-like fields have been considered by Wang & Steinhardt (1998), Iliev & Shapiro (2001) and Lokas & Hoffman (2001). Constraints on Λ at the level of clusters and superclusters have been placed by means of optical gravitational lens surveys (Quast & Helbig 1999) and peculiar velocities of galaxies (Zehavi & Dekel 1999). Other papers (e.g. Axenides et al. 2000, Nowakowski 2001 and Nowakowski et al. 2001) have studied the effect of Λ on galactic structures within the framework of General Relativity, though looking at this effect not in the self-gravitating sources themselves, but through the dynamics of test observers in a Schwarzschild-deSitter field that is supposed to be the “external” field of these sources.

In this paper we complement and extend previous work by studying a spherically symmetric, self-gravitating, Maxwell-Boltzmann (MB) gas in hydrostatic equilibrium with a Λ -field given as a “cosmological constant”, subject to observational constraints. Although galactic halo structures are characterized by Newtonian energies and velocities, we find it to be more correct to examine these sources within General Relativity and then obtain the adequate (“weak field”) Newtonian limit. The reason for this approach follows from the fact that in Newtonian physics the mass density is the only source of gravitation and so a non-gravitational interaction, such as the Λ -field, does not contribute to the “effective gravitational mass”. In General Relativity, on the other hand, all forms of matter-energy count as sources of gravitation (curvature of spacetime). Therefore, even in the Newtonian limit, the matter-energy contribution from the Λ -field could be comparable (or at least might not be negligible in comparison) to rest-mass density of the MB gas, so that the hydrostatic equations furnished by the Newtonian limit might not coincide with those “naively” obtained from a Newtonian framework. As we show in this paper, for a MB gas and a constant Λ -field, the Newtonian limit yields a different set of equilibrium equations from those of Newtonian theory. However, we cannot know *a priori* if this difference leads to significant or negligible effects until we solve the equilibrium equations and compare their solutions in both cases. Such ambiguity regarding the Newtonian limit would not arise if we were only dealing with a MB gas (a thermal source), this is so because in this case the internal energy (the only contribution to matter-energy besides rest-mass) is negligible in comparison with rest-mass, leading to the “isothermal sphere” as the unequivocal Newtonian limit.

It is a well known result that within the hierarchical model of structure formation (White & Rees 1978) the final halo structure which results from the repeated merger events building up a galaxy is well represented not by an isothermal structure, but by a centrally divergent steep inner halo profile, first noted by Navarro, Frenk & White (1997), and since confirmed by numerous authors. However, controversy still surrounds this result in as much as direct dynamical studies of galactic rotation curves, across wide dynamical ranges in galaxy size, appear to indicate the presence of a constant density core in the dark haloes of galaxies (e.g. Burkert & Silk 1997, de Blok, McGaugh & Rubin 2001, Firmani et al. 2001, among others). This being the case, we think it worthwhile to study in depth the modifications a simple isothermal halo suffers in the presence of a dominant λ component, even though this results may prove to

be merely indicative of a case where not just a stable halo is being treated, but including the full merger-driven formation of such a structure. Whatever the correct structure scenario eventually turns out to be, a detailed understanding of the behaviour of the quintessential galactic halo toy model -the isothermal halo- in the presence of an important cosmological λ term, will surely prove valuable.

The organization of the paper is described below. Sections II, III and IV respectively provide the general relativistic formulation for a non-relativistic MB gas, a Λ -field as a zero gradient limit of a quintessence-like scalar field and the equations of hydrostatic equilibrium for these sources. We examine the Newtonian limit of the models in section V, showing that in the equilibrium equations in this limit do not coincide with the corresponding Newtonian equations for the same sources. In section VI we discuss the cut off length scales, r_1 , r_2 , introduced by the Λ -field, comparing them in section VII (by means of rough qualitative arguments) with physically motivated length scales of virialized halo structures (virialization radius and critical radius associated with Antonov instability). In section VIII we review briefly the equilibrium equations for the King halos, while in section IX we use the numerical integration of the various sets of equilibrium equations in order to verify the issues discussed analytically and qualitatively in previous sections: the difference between the Newtonian limit of General Relativity and a pure Newtonian framework and the fact that r_2 is 5–7 times larger than physically motivated length scales. We briefly summarize these results in section X. The paper contains 9 figures obtained from the numerical solution of the equilibrium equations.

2 THE NON-RELATIVISTIC MAXWELL-BOLTZMANN GAS

A relativistic MB gas follows from a Kinetic Theory formalism associated with the equilibrium MB distribution (de Groot et al. 1980). For gas particles of mass m , the parameter of “relativity coldness” is defined as

$$\beta \equiv \frac{m c^2}{k_B T}, \quad (1)$$

where k_B is Boltzmann constant and T is the temperature. The non-relativistic MB gas corresponds to the limit $\beta \gg 1$, leading to the following forms for the energy density ε and pressure p

$$\varepsilon = n \left(m c^2 + \frac{3}{2} k_B T \right) = m c^2 n \left(1 + \frac{3}{2\beta} \right), \quad (2)$$

$$p = n k_B T = \frac{m c^2 n}{\beta}, \quad (3)$$

with the particle number density, n , given by

$$n = \left[\frac{m c}{\sqrt{2\pi\beta\hbar}} \right]^3 \exp \left[\beta \left(\frac{\mu}{m c^2} - 1 \right) \right], \quad (4)$$

where $2\pi\hbar$ is Planck’s constant and μ is the Gibbs function per particle (de Groot et al. 1980), the chemical potential. The MB distribution is a solution of the Einstein-Boltzmann equations, irrespective of whether the gas is collisional or collisionless, its applicability is only restricted by the criterion

of “non-degeneracy” or “dilute occupancy” (Pathria 1972): $\exp(\mu\beta/mc^2) \ll 1$. For typical galactic halo variables, this criterion holds for particle masses complying with $m \gg 60$ eV (Cabral-Rossetti et al. 2002).

Under General Relativity, a spacetime whose source is a self gravitating MB gas can be described by the Momentum–Energy tensor of a perfect fluid

$$T_{\text{MB}}^{ab} = \varepsilon u^a u^b + p h^{ab}, \quad (5)$$

where ε, p follows from equations (2)–(4) and $h^{ab} = u^a u^b + g^{ab}$. Such a spacetime must admit a timelike Killing vector field (Maartens 1996)

$$\beta^a = \beta u^a, \quad (6)$$

so that

$$\dot{u}_a - h_a^b (\ln \beta)_{;b} = 0, \quad (7)$$

where $\dot{u}_a = u_{;b} u^b$ is the 4-acceleration. Condition (6) implies that the spacetime must be stationary (or static if vorticity vanishes), while condition (7) is the “Tolman Law” indicating that equilibrium of a MB gas in General Relativity requires the existence of a nonzero temperature gradient, a specific spacelike gradient that balances the 4-acceleration associated with a stationary frame. In a comoving representation, condition (7) becomes $T\sqrt{-g_{tt}} = \text{const.}$

3 QUINTESSENCE AND THE Λ FIELD

“Dark energy” matter-energy sources are usually represented as a quintessence-like scalar field ϕ with a Momentum–Energy tensor

$$T_{\text{Q}}^{ab} = \phi^{;a} \phi^{;b} - \left[\frac{1}{2} \phi_{;c} \phi^{;c} + V(\phi) \right] g^{ab}, \quad (8)$$

where $V(\phi)$ is the scalar field potential. Since we are not interested in a cosmological quintessence source, but rather in its gravitational interaction with a MB gas at the galactic and galactic cluster scale, it is reasonable to assume that the gradients $\phi_{;a}$ are negligible, hence we can approximate equation (8) by a “cosmological constant” or a Λ -field given by

$$T_{\text{Q}}^{ab} \approx -V(\phi_0) g^{ab} = -\Lambda g^{ab}, \quad (9)$$

equivalent to a source with matter–energy density

$$\begin{aligned} \Lambda &= \Omega_{\Lambda} \rho_{\text{crit}} c^2, \\ \rho_{\text{crit}} &= 1.88 \times 10^{-29} h^2 \text{ gm/cm}^3 \end{aligned} \quad (10)$$

where, according to observational evidence, we can take $\Omega_{\Lambda} \simeq 0.7$ and $h \simeq 0.65$. If there is only gravitational interaction between the MB gas and the Λ field, the conditions

$$T_{\text{Q}}^{ab}{}_{;b} = 0, \quad T_{\text{MB}}^{ab}{}_{;b} = 0, \quad (11)$$

must hold separately. This condition is trivially satisfied for T_{Q}^{ab} given by equation (9).

4 THE FIELD EQUATIONS

In order to model an equilibrium galactic halo structure we will consider spherically symmetric static spacetimes, com-

patible with equations (6) and (7). The metric is then

$$\begin{aligned} ds^2 &= -\exp\left(\frac{2\Phi}{c^2}\right) c^2 dt^2 + \frac{dr^2}{1 - \kappa M/r} + r^2 d\Omega^2 \\ d\Omega^2 &\equiv d\theta^2 + \sin^2 \theta d\phi^2, \end{aligned} \quad (12)$$

where $\Phi = \Phi(r)$, $M = M(r)$ and $\kappa \equiv 8\pi G/c^2$, so that M is given in mass units. The source of equation (12) is the perfect fluid momentum–energy tensor

$$\begin{aligned} T^{ab} &= T_{\text{MB}}^{ab} + T_{\text{Q}}^{ab} = (\varepsilon + \Lambda) u^a u^b + (p - \Lambda) h^{ab}, \\ u^a &= \exp(-\Phi/c^2) \delta^a_t, \end{aligned} \quad (13)$$

with ε, p given by equations (2)–(4). Einstein’s field equations together with the balance law $T_{\text{MB}}^{ab}{}_{;b} = 0$ for equation (12), equations (13) and (17) now take the form

$$M' = (\varepsilon + \Lambda) r^2 / c^2, \quad (14)$$

$$\frac{\Phi'}{c^2} = \frac{\kappa}{2} \frac{M + (p - \Lambda) r^3 / c^2}{r(r - \kappa M)}, \quad (15)$$

$$p' = -(\varepsilon + p) \frac{\Phi'}{c^2}, \quad (16)$$

where a prime denotes derivative with respect to r . Since the 4-acceleration is given by $\dot{u}_a = \Phi'/c^2 \delta_a^r$, the constraint (7) takes the form

$$\frac{\Phi'}{c^2} = \frac{\beta'}{\beta} \Rightarrow \beta = \beta_c \exp\left(\frac{\Phi - \Phi_c}{c^2}\right), \quad (17)$$

where $\beta_c \equiv \beta(0)$ and $\Phi_c \equiv \Phi(0)$. The subscript c will denote henceforth evaluation along the symmetry center $r = 0$. Inserting equations (2), (3) and (4) into equation (16) and using condition (17) yields after some algebra

$$\frac{\mu'}{\mu} = -\frac{\beta'}{\beta} \Rightarrow \frac{\beta \mu}{m c^2} = C_0 = \text{const.}, \quad (18)$$

so that n, ε and p become functions depending only on β (or on Φ via equation (17)). Using equation (18) and re-scaling n with respect to the central rest–mass density $\rho_c = m n_c$, the matter–energy density and pressure for the equilibrium MB gas become

$$\varepsilon = \rho c^2 \left(1 + \frac{3}{2\beta}\right), \quad p = \frac{\rho c^2}{\beta}, \quad (19)$$

where the rest–mass density is given by

$$\frac{\rho}{\rho_c} = \left(\frac{\beta_c}{\beta}\right)^{3/2} e^{\beta_c - \beta}. \quad (20)$$

However, it is more useful to express these state variables and the field equations themselves in terms of the central velocity dispersion (e.g. Binney & Tremaine 1987)

$$\sigma_c^2 \equiv \frac{k_B T_c}{m} = \frac{c^2}{\beta_c}, \quad (21)$$

and the dimensionless variable

$$\Psi \equiv \frac{\Phi_c - \Phi}{\sigma_c^2}, \quad (22)$$

which in the Newtonian limit becomes the “normalized potential”. Combining equations (17), (21) and (22), we obtain the “redshifted” temperature provided by Tolman’s law

$$T = T_c \exp\left(\frac{\Phi_c - \Phi}{c^2}\right) = T_c \exp\left(\frac{\sigma_c^2}{c^2} \Psi\right), \quad (23)$$

showing the specific temperature gradient of an MB gas in thermodynamic equilibrium.

With the help of equations (17) and (20), we obtain

$$\frac{\rho}{\rho_c} = \exp \left[\frac{3}{2} \frac{\sigma_c^2}{c^2} \Psi + \frac{c^2}{\sigma_c^2} \left(1 - e^{-(\sigma_c/c)^2 \Psi} \right) \right], \quad (24)$$

so that ε and p become

$$\varepsilon = \rho c^2 \left[1 + \frac{3}{2} \frac{\sigma_c^2}{c^2} e^{(\sigma_c/c)^2 \Psi} \right], \quad (25)$$

$$p = \rho \sigma_c^2 e^{-(\sigma_c/c)^2 \Psi}, \quad (26)$$

The field equation that we have to solve are then equations (14) and (15), with ε , p and Λ given by equations (10), (25) and (26). However, it is convenient to express these equations in terms of equations (21), (22) and the following dimensionless variables

$$\begin{aligned} x &= \frac{r}{r_0}, & r_0^{-2} &= \frac{4\pi G \rho_c}{\sigma_c^2}, \\ \mathcal{M} &= \frac{M}{\rho_c r_0^3}, \end{aligned} \quad (27)$$

leading to

$$\begin{aligned} \frac{d\mathcal{M}}{dx} &= \left[\frac{\rho}{\rho_c} \left(1 + \frac{3}{2} \frac{\sigma_c^2}{c^2} e^{(\sigma_c/c)^2 \Psi} \right) + \lambda \right] x^2, \\ \frac{d\Psi}{dx} &= - \frac{\mathcal{M} + \left[(\rho/\rho_c) (\sigma_c^2/c^2) e^{(\sigma_c/c)^2 \Psi} - \lambda \right] x^3}{x \left[x - 2 (\sigma_c^2/c^2) \mathcal{M} \right]}, \end{aligned} \quad (28)$$

where ρ/ρ_c follows from equation (24) and

$$\lambda \equiv \Omega_\Lambda \frac{\rho_{\text{crit}}}{\rho_c} = 2.538 \times 10^{-7} \Omega_\Lambda h^2 \frac{M_\odot/\text{pc}^3}{\rho_c}, \quad (29)$$

while the length scale r_0 is one third of the ‘‘King radius’’ of Binney & Tremaine (1987) and can be given numerically as

$$r_0 = 4.2303 \times 10^{-6} \frac{\sigma_c}{\text{km/sec}} \left(\frac{M_\odot/\text{pc}^3}{\rho_c} \right)^{1/2} \text{Mpc}. \quad (30)$$

Now equation (28) is a self-consistent system of differential equations that can be integrated once numerical values for the independent parameters (ρ_c , σ_c , Ω_Λ , h) have been supplied, while regularity conditions at the center require $\mathcal{M}_c = \mathcal{M}'_c = \Psi_c = \Psi'_c = 0$. Notice that by setting $\Omega_\Lambda = 0$, we obtain the general relativistic equations of hydrostatic equilibrium for a Maxwell–Boltzmann gas characterized by the equation of state of equations (2) and (3)–(4).

An alternative system to that of equation (28), that is easier to handle numerically, follows by expressing ρ , ε , p as functions of β by means of equations (19) and (20), so that β replaces Ψ in equation (28). However, the variables \mathcal{M} and Ψ in equation (28) are more convenient to explore the Newtonian limit.

5 THE NEWTONIAN LIMIT VS. NEWTONIAN CONFIGURATIONS

We can identify Newtonian conditions, within the framework of General Relativity, as the weak field limit of the theory

for the metric of equation (12) and source of equation (13). By looking at equations (23), (24), (25)–(26) and (28), dimensionless variables Ψ and \mathcal{M} (which are not, necessarily, small) always appear multiplied by the ratio σ_c^2/c^2 . Since σ_c is a characteristic velocity of the MB gas, we can examine Newtonian conditions by expanding all relevant quantities in powers of this ratio. Using relation (27) we find to first order in σ_c^2/c^2

$$\begin{aligned} \exp \left[\frac{2(\Phi - \Phi_c)}{c^2} \right] &\approx 1 - 2 \frac{\sigma_c^2}{c^2} \Psi, \\ \left[1 - \frac{\kappa M}{r} \right]^{-1} &\approx 1 + 2 \frac{\sigma_c^2}{c^2} \frac{\mathcal{M}}{x}. \end{aligned} \quad (31)$$

Thus, the Newtonian limit of General Relativity for the sources under consideration is characterized by

$$\frac{\sigma_c}{c} \ll 1 \quad \Rightarrow \quad \frac{\Phi}{c^2} \ll 1, \quad \frac{\kappa M}{r} \ll 1, \quad (32)$$

so that $g_{tt} \approx -1$, $g_{rr} \approx 1$ and we can identify (in this limit) the Newtonian potential with Φ . Also, at first order in σ_c^2/c^2 we have

$$\begin{aligned} -\frac{3}{2} \frac{\sigma_c^2}{c^2} \Psi + \frac{c^2}{\sigma_c^2} \left[1 - e^{-(\sigma_c/c)^2 \Psi} \right] &\approx \\ \frac{c^2}{\sigma_c^2} \left[1 - e^{-(\sigma_c/c)^2 \Psi} \right] &\approx \frac{c^2}{\sigma_c^2} \left[1 - \left\{ 1 - \frac{\sigma_c^2}{c^2} \Psi \right\} \right] \approx \Psi, \end{aligned}$$

and so equations (23), (24) and (25)–(26) become

$$\frac{\rho}{\rho_c} \approx e^\Psi, \quad \varepsilon \approx \rho c^2, \quad p \approx \frac{\sigma_c^2}{c^2} \varepsilon \ll \varepsilon, \quad (33)$$

$$T \approx T_c \left[1 - \frac{\sigma_c^2}{c^2} \Psi \right] = T_c \left[1 - \frac{\sigma_c^2}{c^2} \ln \frac{\rho}{\rho_c} \right] \quad (34)$$

thus, a spherical MB gas in its Newtonian limit approaches the ‘‘isothermal sphere’’ with $T = T_c$ (or, equivalently $\sigma = \sigma_c$) for all x (see figure 1). The field equations (28) become (at first order in σ_c^2/c^2) the system

$$\begin{aligned} \frac{d\mathcal{M}}{dx} &= \left[e^\Psi \left(1 + \frac{3}{2} \frac{\sigma_c^2}{c^2} \right) + \lambda \right] x^2, \\ \frac{d\Psi}{dx} &= - \frac{\mathcal{M}}{x^2} - \left(\frac{\sigma_c^2}{c^2} e^\Psi - \lambda \right) x, \end{aligned} \quad (35)$$

where we have kept, together with rest-mass energy density ($\propto \rho$), the other two contributions to the total matter-energy density: internal energy ($\propto p \propto \sigma_c^2 \rho$) and that of the Λ field (λ), as we do not know *a priori* which one of the latter two contributions is larger. In the case without the Λ field ($\lambda = 0$), we only need to compare rest-mass and internal energy densities. From equations (32) and (33), it is evident that in this case the Newtonian limit of equation (35) can only lead to the equilibrium equations for the Newtonian ‘‘isothermal sphere’’

$$\begin{aligned} \frac{d\mathcal{M}}{dx} &= e^\Psi x^2, \\ \frac{d\Psi}{dx} &= - \frac{\mathcal{M}}{x^2}, \end{aligned} \quad (36)$$

whose corresponding Poisson equation is

$$-\frac{1}{x^2} \frac{d}{dx} \left(x^2 \frac{d\Psi}{dx} \right) = e^\Psi. \quad (37)$$

However, if we have the contribution of the Λ field (besides the internal-energy term) then, before deciding which terms can be neglected, we should verify first if λ is comparable in magnitude to the internal energy density term that is first order in σ_c^2/c^2 . This comparison is especially important in the “force” equation (*i.e.* the second of equations (35)) where this term and λ have opposite signs.

For a wide variety of galactic objects (from dwarf galaxies to clusters), we have the range $4 \text{ km/sec} < \sigma_c < 1500 \text{ km/sec}$ (e.g. Kleyna 2002, Wilkinson 2002, Salucci & Burkert 2000), hence

$$10^{-9} < \frac{\sigma_c^2}{c^2} < 2.5 \times 10^{-5}, \quad (38)$$

On the other hand, for currently accepted estimates of central halo density: $0.001 M_\odot/\text{pc}^3 < \rho_c < 1 M_\odot/\text{pc}^3$, (e.g. Firmani et al. 2001, Shapiro & Iliev 2002, Dalcanton & Hogan 2001) we have

$$4 \times 10^{-6} \Omega_\Lambda h^2 < \lambda < 4 \times 10^{-3} \Omega_\Lambda h^2. \quad (39)$$

Therefore, since $\Omega_\Lambda \simeq 0.7$ and $h \simeq 0.65$, it is evident that near the center we have $\rho/\rho_c = e^\Psi \approx 1$ and so σ_c^2/c^2 and λ can have comparable magnitude (especially for structures with large $\rho_c \sim 1 M_\odot/\text{pc}^3$). However, as x increases the λ term remains constant while ρ/ρ_{crit} decreases, implying that for large x the constant λ term will always end up dominating. Also, since the Newtonian potential is negative with $|\Phi_c| > |\Phi|$ so that $\Psi < 0$, we can safely assume that $\lambda \gg (\sigma_c/c)^2 e^\Psi$ holds even for small values of x .

Therefore, we can ignore the contribution from hydrostatic pressure in equations (35) and replace them by

$$\begin{aligned} \frac{d\mathcal{M}}{dx} &= (e^\Psi + \lambda) x^2, \\ \frac{d\Psi}{dx} &= -\frac{\mathcal{M}}{x^2} + \lambda x, \end{aligned} \quad (40)$$

so that

$$-\frac{1}{x^2} \frac{d}{dx} \left(x^2 \frac{d\Psi}{dx} \right) = e^\Psi - 2\lambda. \quad (41)$$

These equations are the Newtonian limit of equation (28), based on removing only those terms that can be neglected for all x in terms of expansions around σ_c^2/c^2 and of comparison with rest-mass density. However, it is interesting to remark that if we start from the Newtonian isothermal sphere, as given by equations (36) and (36), and within a purely Newtonian framework (*ie* not the Newtonian limit of General Relativity) we generalize it by adding a Λ -type repulsive interaction, we would not obtain equations (40) and (41), but the set

$$\begin{aligned} \frac{d\mathcal{M}}{dx} &= e^\Psi x^2, \\ \frac{d\Psi}{dx} &= -\frac{\mathcal{M}}{x^2} + \lambda x, \end{aligned} \quad (42)$$

$$-\frac{1}{x^2} \frac{d}{dx} \left(x^2 \frac{d\Psi}{dx} \right) = e^\Psi - 3\lambda, \quad (43)$$

since in Newtonian gravity the Λ field only enters into the “force” equation in (42) but does not enter in the evaluation of the gravitational mass \mathcal{M} that follows from integrating equation (42). On the other hand, in the Newtonian limit

equations (40) the form of \mathcal{M} (and thus the forms of Ψ and all variables related to \mathcal{M} and Ψ) is affected by the presence of the λ term.

This difference between a purely Newtonian treatment and the Newtonian limit from General Relativity is a significant feature certainly worth remarking, since it concerns M which is the effective gravitational mass affecting the evolution of test observers and light rays. Since General Relativity is currently the best available theory of gravitation, we suggest that the system of equations (40)–(41) should be preferred (at least conceptually) to the purely Newtonian system of equations (42)–(43). In fact, these systems have different solutions and if the differences in these solutions are not negligible, this can (in principle) be relevant in dark matter tracing and gravitational lensing methods used for estimating the properties of dark matter haloes of galactic clusters. The long numerical integrations of cosmological N-body simulations imply that even minor correction factors, of the type discussed here, could have important effects on the final result. Figures 2a and 2b illustrate how the correct Newtonian limit of a Maxwell–Boltzmann gas in equilibrium with a Λ -field is furnished by equations (40)–(41), just as the Newtonian limit without Λ is the isothermal sphere. However, before solving equations (40) and (42) numerically it is not possible to know if the differences in their solutions are significant or negligible. We will examine this issue in section IX (see figures 2 and 3). For the remaining of the discussion we will consider only the Newtonian limit (NL) equations (40).

6 EXISTENCE AND STABILITY OF CIRCULAR GEODESIC ORBITS

The relativistic generalization of the “rotation velocity” along circular orbits is the rotation velocity of test observers along circular geodesics in the spacetime, equation (12). Bounded timelike geodesics of equation (12) are characterized by (Chandrasekhar 1983) $\theta = \pi/2$ and by two constants of motion, “energy” $E_0 = 2e^{2\Phi/c^2} \dot{t}$ and “angular momentum” $L_0 = r^2 \dot{\varphi}$, where the dot denotes derivative with respect to proper time of the observers. Radial motion is governed by

$$\frac{e^{2\Phi/c^2}}{1 - \kappa M/r} \dot{r}^2 + V(r) = E_0^2,$$

where

$$V(r) = e^{2\Phi/c^2} \left(1 + \frac{L_0^2}{r^2} \right),$$

is the “effective potential”. The conditions for the existence of circular geodesic orbits with radius $r = r^*$ are $\dot{r} = \ddot{r} = 0$, leading to

$$E_0^2 = \frac{e^{2\Phi/c^2}}{1 - r\Phi'/c^2}, \quad L_0^2 = \frac{r^3 \Phi'/c^2}{1 - r\Phi'/c^2}, \quad (44)$$

so that

$$\Phi' > 0, \quad 1 - r\Phi'/c^2 > 0, \quad (45)$$

Stability of these orbits requires $r = r^*$ to be a minimum of the effective potential. Hence we must have $V'(r^*) = 0$ and

$V''(r^*) > 0$, leading (with the help of equations (44)) to

$$3\Phi' + r\Phi'' - 2r\Phi'^2/c^2 > 0. \quad (46)$$

Using the full relativistic equilibrium equations (28) and expressing conditions (45) in terms of the variables introduced in section IV, the conditions for the existence of circular geodesic orbits are, up to first order in σ_c^2/c^2 ,

$$\frac{\lambda x^3 - \mathcal{M}}{x^2} - \left[x e^\Psi + \frac{2\mathcal{M}}{x^3} - 2\lambda\mathcal{M} \right] \frac{\sigma_c^2}{c^2} < 0, \quad (47)$$

$$1 + \frac{\lambda x^3 - \mathcal{M}}{x} \frac{\sigma_c^2}{c^2} > 0, \quad (48)$$

while the condition (46) for stability becomes

$$\begin{aligned} & \frac{(3\lambda - e^\Psi)x^3 - \mathcal{M}}{x^2} + \frac{\sigma_c^2}{c^2} \left\{ 4\lambda^2 x^3 + (x^3 e^\Psi - 2\mathcal{M})\lambda \right. \\ & \left. + \left[\frac{(\Psi^2 - 3\Psi - 11)x - 6\mathcal{M}}{2} - 3\mathcal{M} \right] e^\Psi + \frac{2\mathcal{M}}{x^3} \right\} < 0, \end{aligned} \quad (49)$$

In the Newtonian limit we can neglect the terms multiplying σ_c^2/c^2 , hence condition (48) becomes trivial, while conditions (47) and (49) respectively become the Newtonian limit conditions for existence and stability of circular geodesic orbits

$$\mathcal{M} - \lambda x^3 > 0, \quad (50)$$

$$\mathcal{M} - (3\lambda - e^\Psi)x^3 > 0. \quad (51)$$

These conditions coincide with those that would have resulted had we used the Newtonian limit equations (40) (instead of the relativistic equations) in equations (45) and (46). If we had used the Newtonian equations (42) we would have obtained the same existence condition (50) but the stability condition would be condition (51), modified by having the λ term multiplied by a factor of 4, instead of 3. Figures 3a and 3b depict graphically conditions (50) and (51) from the numerical solution of conditions (40) and (42).

The actual velocity of observers along circular geodesics follows from evaluating $d\varphi/dt = \dot{\varphi}/\dot{t}$, which with the help of the previous equations (see Cabral-Rosetti et al. 2002) yields

$$v^2(r) = r\Phi' = -x\sigma_c^2 \frac{d\Psi}{dx} = \sigma_c^2 \left[\frac{\mathcal{M}}{x} - \lambda x^2 \right] \quad (52)$$

where we have used equation (40) to eliminate $d\Psi/dx$. Since Φ becomes the Newtonian gravitational potential in the Newtonian limit, circular geodesics orbits exist and $v(r)$ is well defined as long as the gravitational force field is attractive (*ie* $\Phi' > 0$ or equivalently $d\Psi/dx < 0$).

For physically reasonable spherical configurations, we must demand that existence and stability conditions (50) and (51) (or (59) and (60)), as well as that $v^2 > 0$, should hold at least in a finite range $0 < x < x_\lambda$ around the symmetry center, where x_λ is a radius where one of these conditions breaks down. A sufficient condition for this follows by looking at the behavior of conditions (50) and (51) around the symmetry center. Expanding \mathcal{M} around $x = 0$ with the help of equation (40) and the regularity conditions $\mathcal{M}(0) = \mathcal{M}_x(0) = \Psi(0) = \Psi_x(0) = 0$, where the subindex x denotes derivative with respect to x . We obtain $\mathcal{M} \approx (1/6)\mathcal{M}_{xxx}(0)x^3 = (1 + \lambda)x^3/3$, hence for $x \approx 0$ both conditions (50) and (51) yield $(1 - 2\lambda)x^3/3 > 0$, so

that the central density must satisfy

$$\rho_c > 2\Omega_\Lambda \rho_{\text{crit}}. \quad (53)$$

Had we used the Newtonian equations (42) instead of equation (40), we would have obtained $\rho_c > 3\Omega_\Lambda \rho_{\text{crit}}$, representing a very small departure from the Newtonian limit expression (53).

The fact that physically reasonable configurations require a minimal bound on ρ_c is an interesting result that has no equivalent in the isothermal sphere and the King halos. Since $e^\Psi = \rho/\rho_c$ and setting $\lambda = 0$ in equations (50), (51) and (52), it is evident that stable geodesic circular orbits, of any radius and for any value of $\rho_c > 0$, always exist for the isothermal sphere and the King models (see section VIII) as long as \mathcal{M} and ρ are positive. If there is a Λ -field then for very small central densities violating condition (53), conditions (50) and (51) do not hold in a range around the symmetry center, though these conditions do hold for a set of ranges like $0 < x_i < x < x_j$ (see figure 3c). However, these cases with $\rho_c \leq 2\Omega_\Lambda \rho_{\text{crit}}$ are unphysical and will not be examined any further.

Bearing in mind equations (10) and (29), condition (53) is satisfied by all known virialized galactic structures whose current estimates of ρ_c are between three and six orders of magnitude larger than ρ_{crit} . In fact, the extremely low values $\rho_c < 2\Omega_\Lambda \rho_{\text{crit}}$ would apply today only to large superclusters, still “in-falling” within a linear regime, whose density contrast is of order unity. Obviously such large scale structures cannot be equilibrium configurations (hence the remarks in Nowakowski 2001, Nowakowski et al. 2002 are obvious for present day structures). Moreover, ρ_{crit} is a (model dependent) function of the cosmic era, hence the minimal ρ_c for stable configurations varies with the virialization redshift z_{vir} . Assuming a Λ -CDM model for which $\Omega_{\text{CDM}} + \Omega_\Lambda = 1$, the critical density at any z is given in terms of ρ_{crit} today by

$$\rho_{\text{crit}}(z) = \left[(1 - \Omega_\Lambda)(1 + z)^3 + \Omega_\Lambda \right] \rho_{\text{crit}}(z = 0). \quad (54)$$

Thus, for dwarf galaxies which virialized at large z (*ie* $z_{\text{vir}} < 30$), equations (53) and (54) imply

$$\rho_c(z = 30) > 1.8 \times 10^4 \rho_{\text{crit}}(z = 0) \sim 0.008 M_\odot/\text{pc}^3, \quad (55)$$

a minimal bound on ρ_c that agrees with current estimates (Firmani et al. 2001, Shapiro & Iliev 2002, Kleyna et al. 2002) for central halo densities of these galaxies. Within the current hierarchical models of structure formation, where large structures form as the result of the merger of smaller ones, given Liouville’s theorem, it is clear that the central densities of the first bound structures will also represent an indicative upper bound on the central densities of larger structures. It is interesting that dynamical studies across wide ranges of galactic haloes consistently find central densities above the stability requirement at $z \approx 30$ of $0.008 M_\odot/\text{pc}^{-2}$. Figure 4 illustrates the minimal bound on ρ_c given by condition (55).

7 CUT OFF SCALE OF Λ AND COMPARISON WITH OTHER LENGTH SCALES

Assuming that condition (53) holds, each one of conditions (50) and (51) will necessary break down at some radii, x_1 , x_2 , given by the smallest positive roots of the equations

$$\mathcal{M}(x_1) - \lambda x_1^3 = 0, \quad (56)$$

$$\mathcal{M}(x_2) - [3\lambda - e^{\Psi(x_2)}]x_2^3 = 0. \quad (57)$$

These radii provide “cut off” length scales that do not exist when $\lambda = 0$. We will compare these length scales with other physical cut off scales, such as the virialization radius and the radius for the onset of Antonov instability.

It is useful to express conditions (50) and (51) in terms of the volume average of rest–mass energy density ρ . Under Newtonian conditions the total matter–energy density is $\varepsilon_{\text{total}} = (\rho + \Omega_\Lambda \rho_{\text{crit}}) c^2$, while its volume average is

$$\begin{aligned} \frac{\langle \varepsilon_{\text{total}} \rangle}{c^2} &= \frac{4\pi \int_0^r (\rho + \Omega_\Lambda \rho_{\text{crit}}) r^2 dr}{4\pi \int_0^r r^2 dr} = \frac{3M}{r^3} \\ &= \langle \rho \rangle + \Omega_\Lambda \rho_{\text{crit}}, \end{aligned} \quad (58)$$

therefore, conditions (50) and (51) can be given respectively as

$$\langle \rho \rangle > 2\Omega_\Lambda \rho_{\text{crit}}, \quad (59)$$

$$\frac{1}{4} \langle \rho \rangle + \frac{3}{4} \rho > 2\Omega_\Lambda \rho_{\text{crit}}, \quad (60)$$

where we used equation (29) and $M/r^3 = \rho_c \mathcal{M}/x^3$. Equations (56) and (57) then become

$$\langle \rho \rangle(x_1) = 2\Omega_\Lambda \rho_{\text{crit}}, \quad (61)$$

$$\frac{1}{4} \langle \rho \rangle(x_2) + \frac{3}{4} \rho(x_2) = 2\Omega_\Lambda \rho_{\text{crit}}, \quad (62)$$

From the volume averaging definition (58), we obtain by integration by parts

$$\langle \rho \rangle = \frac{\int \rho x^2 dx}{\int x^2 dx} = \rho - \frac{\int x^3 \rho_x dx}{x^3} \quad (63)$$

Hence, for $0 < x < x_\lambda$, where $x_\lambda = r_0 x_\lambda$ is either one of x_1 , x_2 , we have: $\langle \rho \rangle \geq \rho$. Since condition (59) holds in this range, then $\rho_x < 0$ follows from $\Psi_x < 0$ (because $\rho_x \propto \Psi_x \exp(\Psi)$). Therefore for any x in the range of interest we have $(1/4) \langle \rho \rangle + (3/4) \rho \geq \langle \rho \rangle$. Hence, the root x_2 corresponds to larger density values than x_1 , but since both ρ and $\langle \rho \rangle$ decrease with x , we must necessarily have

$$x_2 \leq x_1, \quad (64)$$

which is a reasonable result, since it is to be expected that the repulsive Λ -field will destabilize those circular orbits with radii $x_2 < x < x_1$ that lie near the length scale x_1 beyond which no such orbits exist. As we show in section IX, the range $x_2 < x < x_1$ corresponds to a transition zone between the isothermal region $0 < x < x_2$ and the asymptotic region $x > x_1$ dominated by the Λ -field. Thus, since $x = x_2$ marks the maximal radius of a stable circular orbit, we can consider this radius as a “cut off” scale for isothermal spheres in hydrostatic equilibrium with a Λ -field. In the remaining of this section we will use simple qualitative arguments to compare other cut off length scales of the isothermal sphere with x_1 . Since numerical estimates (see figure 5a) show that x_2 is about two thirds of x_1 (see section IX), this comparison can be extended to x_2 as well.

Consider the virialization radius, r_{vir} , the currently accepted physical cut off scale associated with the virialization of galactic structures (Padmanabhan 1995). The condition to determine the value of this length scale follows from the Newtonian spherical “in fall” (or “top hat”) model as Lokas & Hoffman (2001), Iliev & Shapiro (2001) and Padmanabhan (1995) show,

$$\langle \rho \rangle(r_{\text{vir}})|_{z_{\text{vir}}} \approx \Delta \rho_{\text{crit}}(z_{\text{vir}}), \quad (65)$$

or, equivalently (using equations (27) and (58)), as

$$\frac{\mathcal{M}(x_{\text{vir}})|_{z_{\text{vir}}}}{x_{\text{vir}}^3} \approx \frac{\Delta + \Omega_\Lambda}{3} \frac{\rho_{\text{crit}}(z_{\text{vir}})}{\rho_c(z_{\text{vir}})}, \quad (66)$$

where the factor Δ is a model dependent (see Lokas & Hoffman 2001 for a discussion on this issue) contrast factor between the average rest–mass density of the overdense region and the critical density of the cosmological background, both evaluated at a virialization epoch, $0 < z_{\text{vir}} < 30$, which depends on the galactic structure and/or a specific structure formation model. From equations (61) and (65), we can see that both $\langle \rho \rangle(r_1)$ and $\langle \rho \rangle(r_{\text{vir}})$ are proportional to ρ_{crit} . Therefore, for all $z < z_{\text{vir}}$, once the galactic structure has virialized and the equilibrium equations are valid, we have

$$\frac{\langle \rho \rangle(r_1)}{\langle \rho \rangle(r_{\text{vir}})} \approx \frac{2\Omega_\Lambda}{\Delta}, \quad (67)$$

or the same expression with a factor 3 instead of 2 if we had used the Newtonian equations (42). Since it is reasonable to assume (to a good approximation) that $\langle \rho \rangle \sim \rho \sim r^{-2}$ for $r < r_1$, a rough qualitative estimate of the ratio r_1/r_{vir} is

$$\frac{r_1}{r_{\text{vir}}} \sim \left[\frac{\Delta}{2\Omega_\Lambda} \right]^{1/2}, \quad (68)$$

Considering that $\Delta \sim 100$ in the case when the cosmological background complies with $\Omega_{\text{CDM}} + \Omega_\Lambda = 1$ (Lokas & Hoffman 2001), this estimate means that for present day virialized structures r_1 is approximately one order of magnitude larger than r_{vir} . Because of equation (64), r_2 should be less than an order of magnitude larger than r_{vir} . The precise numerical value of x_{vir} is displayed in figure 5b, while the qualitative estimates mentioned before are corroborated numerically in figures 6 and 7, showing that r_2 is about seven times larger than r_{vir} . Using the Newtonian equations (42) yields smaller r_1 and r_2 by a factor of $\sqrt{2/3}$. In either case, these results indicate that the Λ -field should have a negligible effect on the virialization process.

Another physically motivated length scale, characteristic of the isothermal sphere, is the critical radius associated with the Antonov instability, or with the onset of the gravothermal catastrophe. This radius follows from demanding that the structural parameters of an isothermal sphere should correspond to a stable thermal equilibrium, characterized by a second variation of a suitably defined entropy functional. As discussed in Padmanabhan (1990), for all isothermal spheres extending up to a critical radius R so that E is the Newtonian total energy at R , the constraint $RE/(GM^2) > -0.335$ must hold, though stable configuration with local maxima must also satisfy $\rho_c < 709 \rho(R)$, while isothermal spheres complying with $RE/(GM^2) > -0.335$ but for which $\rho_c/\rho(R) > 709$ correspond to metastable configurations in which the entropy extrema is a saddle point. The critical radius R complies

with

$$\frac{\rho_c}{\rho(R)} = 709, \quad (69)$$

corresponding to the maximal stable isothermal sphere for which entropy is a local maximum. Using equation (29), we can find the ratio

$$\frac{\rho(R)}{\rho_{\text{crit}}} = \frac{5.55 \times 10^3}{h^2} \frac{\rho_c}{M_{\odot}/\text{pc}^3}, \quad (70)$$

which can be compared to the ratio of $\langle \rho \rangle(r_{\text{vir}})$ to ρ_{crit} given by equation (67). This yields approximately

$$\frac{\langle \rho \rangle(r_{\text{vir}})}{\rho(R)} \sim \frac{\rho(r_{\text{vir}})}{\rho(R)} \sim \frac{h^2 \Delta}{5.55 \times 10^3} \frac{M_{\odot}/\text{pc}^3}{\rho_c}, \quad (71)$$

but, if $R < r_1$, then we should have approximately $\langle \rho \rangle \sim \rho \sim r^{-2}$ for $r < R$, hence we obtain a ratio

$$\frac{R}{r_{\text{vir}}} \sim \frac{h \Delta^{1/2}}{74.16} \left(\frac{M_{\odot}/\text{pc}^3}{\rho_c} \right)^{1/2}, \quad (72)$$

and also the following ratio analogous to (68)

$$\frac{r_1}{R} \sim \frac{74.16}{(2\Omega_{\Lambda})^{1/2} h} \left(\frac{\rho_c}{M_{\odot}/\text{pc}^3} \right)^{1/2}. \quad (73)$$

Assuming that $h = 0.65$, $\Omega_{\Lambda} = 0.7$, equations (72) and (73) show that for values (consistent with current estimates) around $\rho_c \sim 10^{-3} - 10^{-2} M_{\odot}/\text{pc}^3$ (see figures 5 and 6), the virialization radius is about the same order of magnitude as the length scale R of equation (69) and about one to two orders of magnitude smaller than r_1 . An estimate of the value of R in Mpc follows from the fact that the variables (27) that we use coincide (save notation differences, a minus sign in Ψ) with those defined in equations (4.21) and (4.22) of Padmanabhan (1990) which yield $x(R) = R/r_0 = 34.2$. Using equation (30) we obtain

$$r(R) = 1.467 \times 10^{-4} \frac{\sigma_c}{\text{km/sec}} \left(\frac{M_{\odot}/\text{pc}^3}{\rho_c} \right)^{1/2} \text{Mpc}. \quad (74)$$

By looking at the numerical solutions for the equilibrium equations (40) and (42), we will verify in section IX the qualitative estimates of r_1, r_2, r_{vir} and R that we have presented above. These estimates tend to support the conclusion that the effects of a Λ field can be ignored in the study of virialized structures.

8 THE KING MODELS

It is interesting to compare the effect of a Λ -field on a MB distribution with other distribution functions (but without Λ). We examine briefly the case of the Michie–King models, obtained by truncation of the MB distribution at a given maximal escape velocity (Binney & Tremaine 1987). This distribution functions leads to equilibrium equations similar to (36), but with ρ/ρ_c given by Binney & Tremaine (1987) and Katz (1980)

$$\frac{\rho}{\rho_c} = \frac{K(\tilde{\Psi})}{K(\Psi_0)}, \quad (75)$$

$$\tilde{\Psi} \equiv \Psi + \Psi_0, \quad \Psi_0 \equiv \frac{\Phi_b - \Phi_c}{\sigma_c^2}, \quad (76)$$

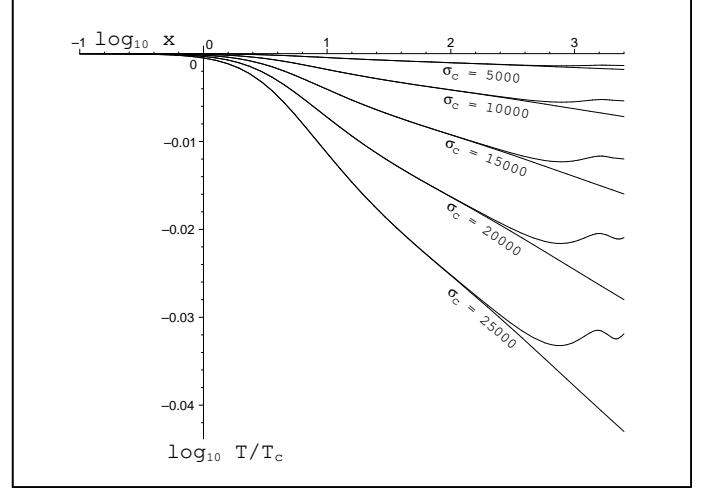


Figure 1. Each pair of curves provides the radial temperature variations within a MB sphere characterized by a given central velocity dispersion (values indicated in km/sec). The curves showing monotonous decay correspond to $\lambda = 0$. In the case with nonzero cosmological λ term, the temperature curves stop decreasing and oscillate around a constant temperature (see text). It is evident that as the velocity dispersion of the halo decreases, the halo tends to an isothermal configuration, valid to a high degree in any astrophysical structure, $\sigma_c < 1000$ km/sec.

$$K(X) = e^X \text{erf}(X^{1/2}) - \frac{2X^{1/2}}{\sqrt{\pi}} \left(1 + \frac{2}{3}X \right), \quad (77)$$

where Ψ is given by equation (22), while $\Phi_b \equiv \Phi(x_b)$ for $x = x_b$ satisfying the constraint $K(x_b) = 0 \Rightarrow \rho(x_b) = 0$. The x_b is known as the “tidal radius” marking a theoretical cut off scale whose value depends on Ψ_0 . The equilibrium equations for the King models expressed in terms of the dimensionless variables x and \mathcal{M} are then

$$\begin{aligned} \frac{d\mathcal{M}}{dx} &= x^2 \frac{K(\tilde{\Psi})}{K(\Psi_0)}, \\ \frac{d\Psi}{dx} &= -\frac{\mathcal{M}}{x^2}. \end{aligned} \quad (78)$$

Since $\tilde{\Psi}(0) = \Psi_0$ and $\mathcal{M}(0) = 0$, the integration of these equations requires one to specify a given value of Ψ_0 , leading to a family of numerical solutions parametrized by Ψ_0 . Theoretical studies of the King distribution applied to globular clusters (see Katz 1980) yield the stability range $\Psi_0 < 8$, though there are observations and theoretical estimates allowing for values up to $\Psi_0 \approx 11$.

As we will show in the following section, the dynamical variables of the King models behave asymptotically in a very different manner from those of the MB models with Λ . However, the cut off scale r_{λ} in the latter is of the same order of magnitude as the tidal radius of King models with deep potential wells ($\Psi_0 \sim 10$).

9 NUMERICAL ANALYSIS

We solve numerically the systems of equations (28), (36), (40), (42) and (78), assuming the regularity conditions

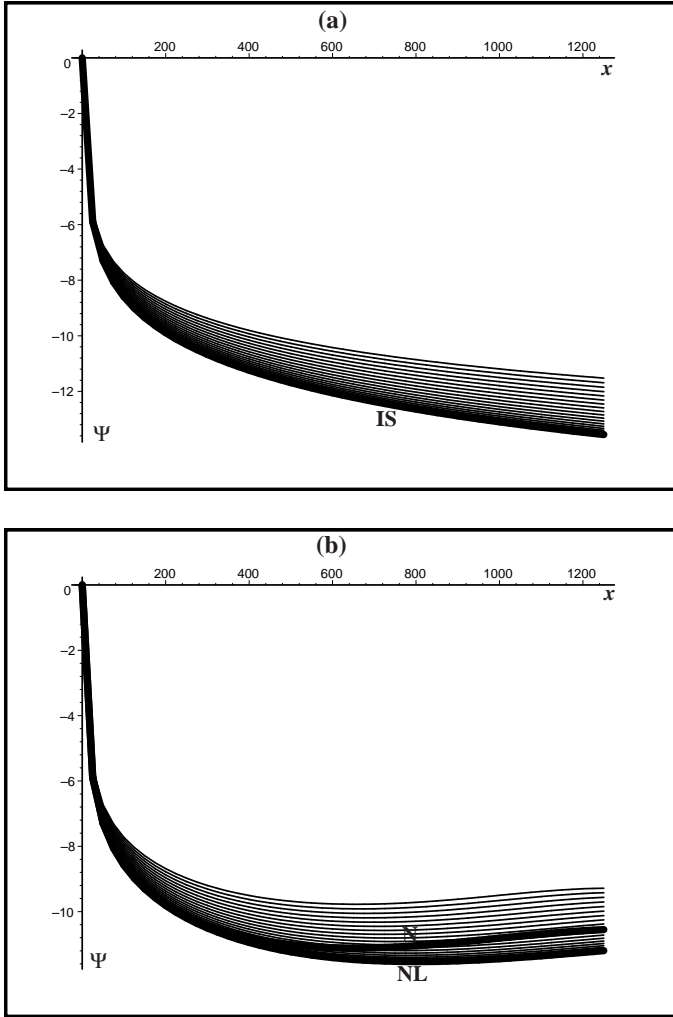


Figure 2. a) Relative potential vs. radius, for MB spheres in the absence of a λ term. The curves are characterized by sequentially decreasing central velocity dispersions, ranging from relativistic values (upper curves) to newtonian values (lower curves). The solid curve at the bottom corresponds to the classical isothermal sphere solution. As the central velocity dispersion decreases the sequence accurately converges to the isothermal sphere. b) Same as panel (a), but in the presence of a cosmological λ term. The curves converge to the solid curve marked NL associated with equations (40), hence it is clear that this is the correct Newtonian limit for the MB spheres obtained from the full General Relativity treatment. The curve marked N corresponds to the naive Newtonian limit associated with equation (40). It is evident that this is not the correct newtonian limit of the MB sphere when there is a Λ -field.

$\mathcal{M}_c = \mathcal{M}'_c = \Psi_c = \Psi'_c = 0$, for $\Omega_\Lambda = 0.7$, $h = 0.65$ and suitable values of the free parameters σ_c , ρ_c , Ψ_0 .

9.1 The isothermal limit with a Λ field

It is interesting to examine the Newtonian limit of the MB gas (with and without the Λ -field) by looking at how an isothermal behavior emerges as temperature gradients decrease for sequentially decreasing values of the ratio σ_c/c , starting from relativistic values down to smaller Newtonian velocities. Using Ψ from the numerical solution of equa-

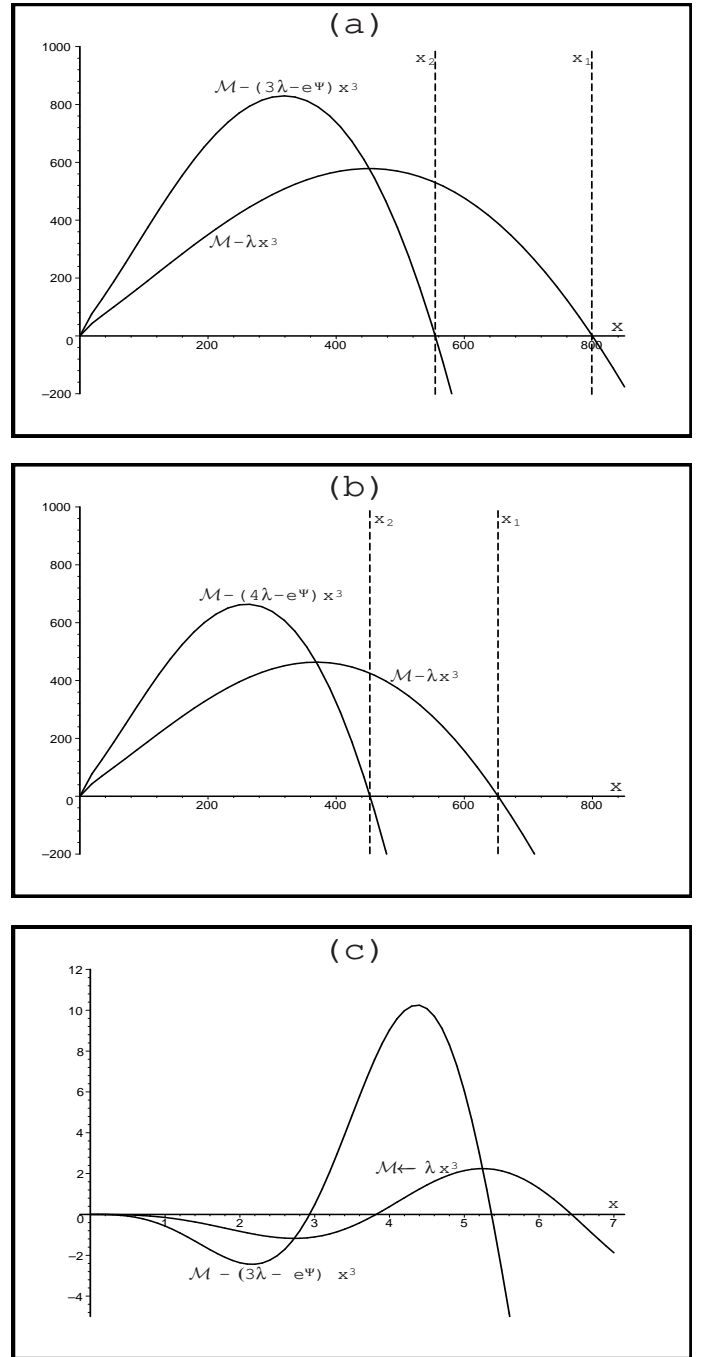


Figure 3. Values of the existence ($M - \lambda x^3$) and stability ($M - (3\lambda - e^\Psi)x^3$) conditions for circular orbits vs. the dimensionless radial coordinate x for MB spheres with $\rho_c = 0.01M_\odot/\text{pc}^3$. Panels (a) and (b) respectively depict the cases of the Newtonian limit and the naive Newtonian treatment. In the latter case the existence and stability radii are about two thirds smaller than those of (a). Panel (c) For depicts the case where central density is lower than the threshold $\rho_c > 2\Omega_\Lambda$. In this case no central structure can exist, as the existence and stability conditions are only met in disconnected ranges not including the origin.

tion (28), we plot in figure 1 the normalized temperature, T/T_c , given by equation (23) vs $\log_{10} x$ for four values in the range $\sigma_c/c = 0.08$ down to $\sigma_c/c = 1.6 \times 10^{-2}$, that is from $\sigma_c = 25000$ km/sec to $\sigma_c = 5000$ km/sec (still a dispersion velocity much larger than that of any galactic structure). As shown in this figure, the temperature gradients of the MB gas are already small ($T/T_c < 0.2$) even for $\sigma_c = 25000$ km/sec, suggesting that even for more relativistic values of σ_c/c the linearized expression (34) can be used instead of equation (23). These gradients steadily decrease for smaller σ_c/c , becoming negligible for the velocities characteristic of galactic structures, and so approaching in the limit $\sigma_c/c \rightarrow 0$ an isothermal condition $T = T_c$. In the case $\Lambda = 0$ the temperature curves steadily decrease so that $T/T_c \rightarrow 0$ as $x \rightarrow \infty$. However, if there is a Λ -field, then these curves stop decreasing at $x = x_1$ and begin to oscillate around a constant value, $T = T_\lambda$, that can be identified as a characteristic temperature of the Λ -field.

9.2 The correct Newtonian limit

The Newtonian limit of equation (28) can also be illustrated by means of sequences of curves corresponding to Ψ obtained from equation (28) for sequentially decreasing values of σ_c/c . The curves of figure 2a ($\lambda = 0$) clearly tend to the thick curve at the bottom, marked as “IS”, corresponding to Ψ for the isothermal sphere, obtained from equation (36). In figure 2b we consider the case with nonzero λ given by equation (29). It is evident that the sequence of curves tends to the thick curve, marked NL, corresponding to Ψ obtained from equation (40) and not to the thick curve, marked “N”, that corresponds to Ψ obtained from equation (42). Hence, the correct Newtonian limit of a MB gas with a Λ field is given by equations (40)–(41) and not by the Newtonian equations (42)–(43).

9.3 The “cut off” length scales

Numerical solution of the systems (40) and (42) allow us to depict graphically conditions (50)–(51) (figures 3a and 3b), conditions (59)–(60) giving the same results, where the length scales for the existence and stability of circular orbits, x_1 and x_2 , follow from the roots given by equations (56)–(57) and (61)–(62). Assuming $\rho_c = 0.01 M_\odot/\text{pc}^3$, the following numerical values emerge from figure 3a: $x_1 \approx 800$, $x_2 \approx 555$, while for the Newtonian equations (42) we obtain smaller values (see figure 3b): $x_1 \approx 660$, $x_2 \approx 460$. For the same value of ρ_c and for the Newtonian limit equations (40) we obtain from figure 5: $x_{\text{vir}} \approx 72$ and $x(R) \approx 35$. These values of x can be translated into actual distances for specific galactic structures by using $r = r_0 x$ where r_0 is given by equation (30). The resulting length scales are shown in Table 1.

As we mentioned in section VI, the conditions (50)–(51) for the existence and stability of circular geodesic orbits are violated for $\rho_c < 2\Omega_\Lambda \rho_{\text{crit}}$. This possibility is illustrated by figure 3c, where these conditions are plotted for $\rho_c = \Omega_\Lambda \rho_{\text{crit}}$, clearly showing how conditions (50)–(51) do not hold around the center (though they do hold in disconnected ranges of x that exclude the center). Since both ρ_c and ρ_{crit} are functions of the cosmic era, condition (53)

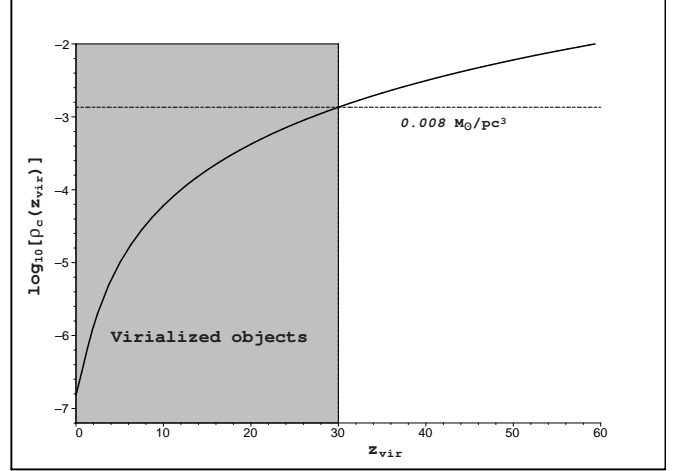


Figure 4. The solid curve shows the minimum central density for stability as a function of virialization redshift. The value at $z = 30$, corresponding to $\rho_c = 0.01 M_\odot \text{pc}^{-2}$, is of the order of observed values in galactic structures which can be thought of as having formed at around that time or less.

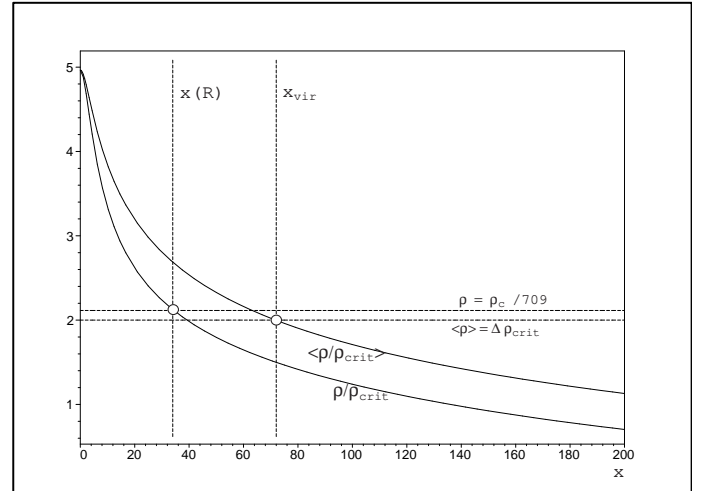


Figure 5. Logarithmic plots of the density and average density vs. dimensionless radius x , both normalized by ρ_{crit} . The intersects with the horizontal dotted lines define the onset of Antonov instability ($\rho = \rho_c/709$) and the virial radius ($\langle \rho \rangle = \Delta \rho_{\text{crit}}$).

with the help of equation (54) yields a minimal bound of ρ_c for virialized structures complying with conditions (50)–(51). This is illustrated in figure 4, showing that structures of relatively recent virialization easily meet this minimal bound, though for galaxies which virialized at $z \sim 30$, the fulfillment of condition (53) is non-trivial, leading to $\rho_c > 0.008 M_\odot/\text{pc}^3$, a value that is consistent with current estimates of ρ_c .

In figures 3a–b and 5 we considered $\rho_c = 0.01 M_\odot/\text{pc}^3$. In order to find out the dependence of the values of x_1 , x_2 and R on ρ_c , we plot in figure 6 the ratios of these length scales with respect to x_{vir} , clearly emerging from this figure that x_1 and x_2 have a very weak dependence on ρ_c and are, respectively, about 10 and 7 times larger than x_{vir} (for the Newtonian case these figures are about two thirds smaller). However, R is quite sensitive to ρ_c , with $x_{\text{vir}} \sim R$ for densi-

Length scale	Dwarf galaxy	Large galaxy	Cluster
Existence of circular orbits, r_1	140 kpc	5 Mpc	32 Mpc
Largest stable circular orbit, r_2	90 kpc	3 Mpc	22 Mpc
Virial radius, r_{vir}	14 kpc	300 kpc	3 Mpc
Antonov instability, R $\rho_c = 0.01 M_\odot/\text{pc}^3$	8 kpc	140 kpc	1.3 Mpc
Antonov instability, R $\rho_c = 0.001 M_\odot/\text{pc}^3$	15 kpc	330 kpc	3.2 Mpc

Table 1. Length scales for galactic structures. Dwarf and large galaxies and clusters are respectively characterized by $\sigma_c = 3, 200, 1000 \text{ km/sec}$. The length scales r_1, r_2 and r_{vir} were evaluated for $\rho_c = 0.01 M_\odot/\text{pc}^3$. See also figures 6 and 7.

ties in the range $0.001 - 0.01 M_\odot/\text{pc}^3$. This is a nice result, illustrating that these two physically motivated length scales approximately coincide for values of ρ_c close to current estimates. All length scales we have considered show a clear linear dependence on σ_c (from equation (30)). This is shown in figure 7, displaying the graph of each length scale as a function of σ_c for a wide range of values of ρ_c ($10^{-5} - 1 M_\odot/\text{pc}^3$). Since the dependence on ρ_c is very weak, the strip of lines for all values of ρ_c simply makes the lines thicker.

9.4 Density profiles and rotation curves

The effects of the Λ -field can be clearly illustrated by plotting relevant physical variables of the isothermal halos, such as the density profiles and rotation velocity along circular orbits.

Figure 8 depicts a logarithmic plot of the rest-mass density, ρ , normalized by ρ_{crit} for $\rho_c = 0.01 M_\odot/\text{pc}^3$, in comparison with the rest-mass density of the isothermal sphere and of King halos associated with various values of Ψ_0 (only the Newtonian limit “NL” case is shown). It is evident that in the range $0 < x < x_2$ where stable circular orbits exist, the density curve of the NL case is almost identical with that of the isothermal sphere (marked as “IS”). However, in the asymptotic range $x > x_1$, these curves are completely different, since for the IS ρ simply decays as x^{-2} while in the NL case it oscillates around a value close to ρ_{crit} . Since $\rho = \rho_c e^\Psi$, these oscillations mark relative maxima and minima of the Newtonian potential, hence $x = x_1$ marks an unstable equilibrium where this potential becomes repulsive (though further out it alternates from repulsive to attractive). Clearly, this behavior of the asymptotic region is dominated by the Λ -field and is in stark contrast with the behavior of the isothermal region $0 < x < x_2$. The region $x_2 < x < x_1$, where circular orbits exist but are unstable, is a transition zone between the isothermal and asymptotic zones. However, in the physical range $0 < x < x_{\text{vir}}$, the effects of the Λ -field are practically negligible. Notice that ρ for the NL case is also very different from the density curves of the King halos, though the cut off boundary (the tidal

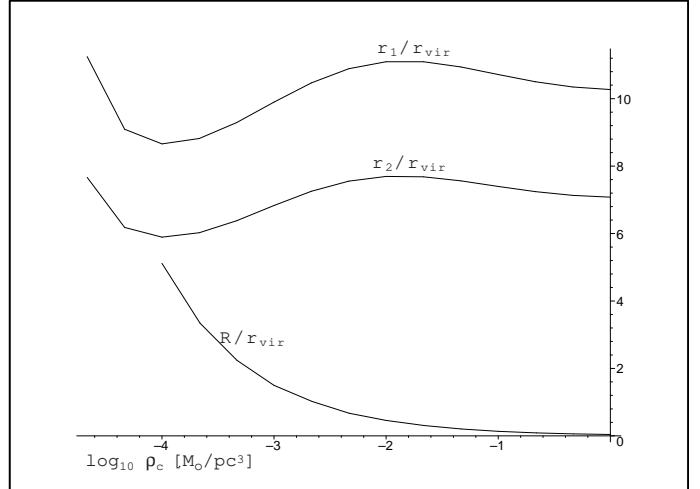


Figure 6. Dependence of circular orbits existence and stability radii, r_1 and r_2 , and onset of Antonov instability, R , all in units of the virial radius, as functions of the logarithm of central density. It is evident that both r_1 and r_2 depend only very weakly on ρ_c and are always well beyond the virial radius. The radius R is much more sensitive to central density, being rather small for larger ρ_c . Since a heat conduction mechanism (interaction cross-section) is required for this mechanism to operate, it probably does not play a significant role.

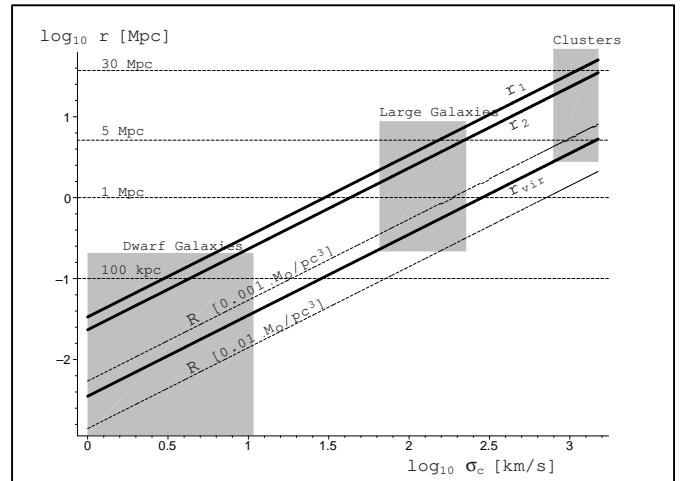


Figure 7. The plot depicts the relation between the indicated radii vs. velocity dispersion, where we have marked with shaded regions the zones occupied by various astrophysical structures. The solid lines represent existence, stability and virial radii for a wide range of central densities. The dotted lines correspond to radii for the onset of Antonov instability for the two indicated values of the central density.

radius) of some of these halos ($\Psi_0 > 10$) can be of the same order of magnitude (or even larger) than x_2 .

Rotation velocities normalized by σ_c are given by equation (52). These “rotation curves” are plotted in figure 9 for the NL case for $\rho_c = 0.01 M_\odot/\text{pc}^3$, in comparison with rotation curves of the isothermal sphere and of King halos associated with various values of Ψ_0 . The figure also displays the cut off length scales x_1, x_2 , separating the isothermal, asymptotic and transition zones, as well as the physical ra-

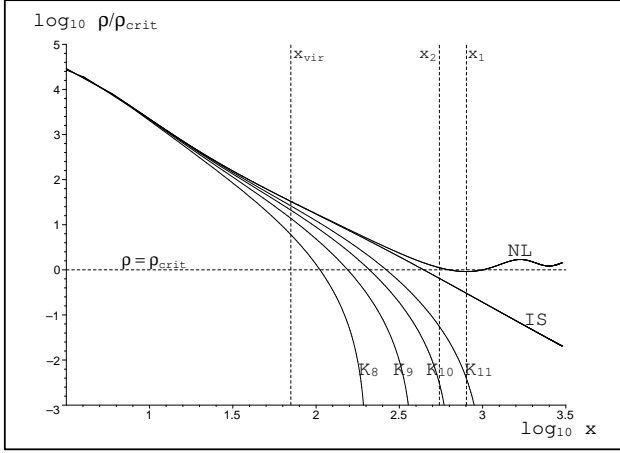


Figure 8. Density profiles normalized by ρ_{crit} as functions of the dimensionless radius x . Curves labeled by **K8** to **K11** give classical King profiles of the indicated shape parameter, **IS** is the isothermal sphere, and **NL** corresponds to the newtonian limit of an MB gas in the presence of a cosmological λ term. Vertical dotted lines indicate the virial radius and the radii for stability and existence of circular orbits.

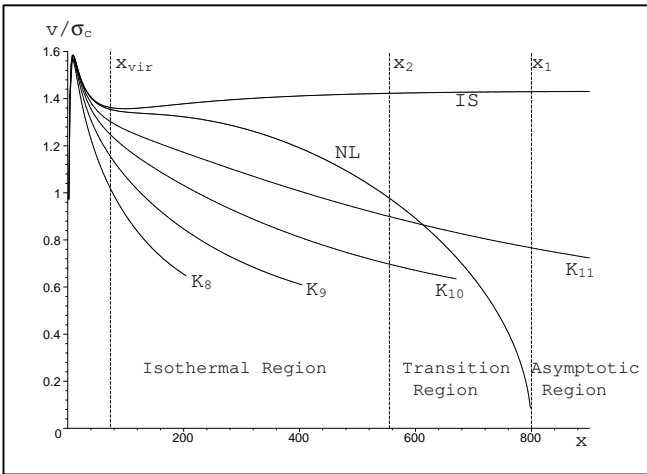


Figure 9. Rotation velocity curves for the cases shown in figure 8. The graphs illustrate that within the Isothermal region, **NL** follows **IS** to within a factor of 1.4, however, within the Transition region, the **NL** rotation curve falls to zero. (see text)

dius x_{vir} . Since this is not a logarithmic plot, the effects of the Λ -field are more noticeable. For example, in the NL case the rotation curve is not flat and decreases significantly already in the isothermal region, though it is practically identical to the rotation curve of the isothermal sphere in the range $0 < x < x_{\text{vir}}$ where all visible matter would be located. The rotation curve of the NL case plunges to zero for $x = x_1$, so that for a range of values $x > x_1$ circular geodesic orbits do not exist. This is connected to the fact that $x = x_1$ marks an unstable equilibrium where the Newtonian potential becomes repulsive. However, this potential oscillates, hence it becomes again attractive and then repulsive again, all of this in disconnected domains of x for $x > x_1$. As a comparison, the rotation curves of King halos (evaluated up to their tidal radii) also decrease but never reach zero.

10 CONCLUSION

We have examined the equilibrium of a MB gas in the presence of a Λ -field constrained by recent observational data. Proceeding from a general relativistic framework and carefully taking the Newtonian limit, we obtain the equilibrium equations (40)–(41) that are different from those that follow from a “naive” Newtonian treatment that would simply add the Λ -field to an isothermal sphere (i.e. equations (42)–(43)). We have shown that the presence of this repulsive field implies that isothermal configurations are now characterized by the length scales, x_1 , x_2 , defined by conditions (50) and (51) and respectively associated with existence and stability of circular geodesic orbits. We have shown that these length scales can also be characterized by the constraints given by (59) and (60) on the rest-mass density and its volume average, hence $x_2 \leq x_1$. The fulfillment of the existence and stability constraints in a region containing the symmetry center $x = 0$ yields a minimal central rest-mass density $\rho_c = 2\Omega_\Lambda \rho_{\text{crit}}$, and thus a minimal central density of $\rho_c = 0.008M_\odot/\text{pc}^3$ for galactic structures having virialized at $z \sim 30$. Since $x = x_2$ marks the radius of the largest stable circular orbit, it is reasonable to consider this radius as the cut off length scale of isothermal configurations in equilibrium with a Λ -field. The numerical solution of the equilibrium equations provides precise numerical estimates of all involved length scales, showing that x_2 is about 7 times larger than physically motivated cut off length scales of isothermal halos, such as the virialization radius x_{vir} and the radius for the onset of Antonov instability R . By looking at the graphs of the rest-mass density and rotation curves, we can identify isothermal ($0 < x < x_2$), asymptotic ($x > x_1$) and transition ($x_2 < x < x_1$) regions in which these variables change from an almost isothermal behavior to an asymptotic regime dominated by the Λ -field. It is quite noticeable that up to the physical cut off scale, x_{vir} , the behavior of the MB gas with the Λ -field is practically indistinguishable from that of an isothermal sphere. Therefore, for the purposes of studying the equilibrium state of virialized structures, the effects of the Λ -field are negligible and can be safely ignored. However, these effects might be important in the study of the gravitational clustering of larger structures that have already left the linear regime but are not yet virialized, or the formation of galactic structures (though the assumption of thermodynamical equilibrium might not be applicable in these cases).

Finally, the zero gradient approximation associated with the constant Λ -field is basically a toy model of more general quintessence-like sources described by non-trivial scalar fields. The equilibrium of a MB gas together with such a source could yield interesting features that are absent in the Λ -field approximation. This problem is currently under investigation (Núñez, Matos and Sussman, 2003).

11 ACKNOWLEDGMENTS

XH acknowledges financial support from **CoNaCyT** grant **I39181-E**. RAS is thankful to Offer Lahav for his warm hospitality and illuminating discussions. RAS also acknowledges inspiration from the wise meowing of his feline friends Moquis, Tontis and Niña.

REFERENCES

- Axenides, M., Floratos, E. G., Perivolaropoulos, L., 2000, *Mod.Phys.Lett.* **A15**, 1541-1550
- Galactic Dynamics*, Binney, J. and Tremaine, S., 1987, Princeton University Press
- Burkert A., Silk J., 1997, *ApJ*, 488, 55
- Cabral-Rosetti, L. G. et al, 2002, *Class Quant Grav*, **19**, 3603-3615
- The Mathematical Theory of Black Holes*, Chandrasekhar, S., 1983, Oxford University Press
- Dalcanton, J. J., Hogan, C. J., 2001, *ApJ*, 561, 35
- de Blok, W. J. G., McGaugh, S. S., Rubin, V. C., 2001, *AJ*, 122, 2396
- Firmani, C., D’Onghia, E. D., Chincarini, G., Hernandez, X., Avila-Reese, V., 2001, *MNRAS*, 321, 713
- Relativistic Kinetic Theory*, de Groot, S. R., van Leeuwen, W. A. and van Weert, Ch. G., 1980, North Holland Publishing Co.
- Iliev, I. T. and Shapiro, P. R., 2001, *MNRAS*, **325**, 468
- Katz, J., 1980, *MNRAS*, **190**, 497
- Kleyna, J., Wilkinson, M. I., Evans, N. W., Gilmore, G., Frayn, C., 2002, *MNRAS*, 330, 792
- Lahav, O., Lilje, P. B., Primack, J. R. and Rees, M. J., 1991, *MNRAS*, **251**, 128
- Lokas, E. L. and Hoffman, Y., 2003, *Non-linear evolution of spherical perturbation in a non-flat Universe with cosmological constant*, astro-ph/0108283
- Causal Thermodynamics in Relativity*, Maartens, R., 1996, Lectures given at the Hanno Rund Workshop on Relativity and Thermodynamics, Natal University, Durban, S.A., June 1996. Available at LANL archives astro-ph/9609119.
- Navarro, J. F., Frenk, C. S., White, S. D. M., 1997, *ApJ*, 490, 493
- Nowakowski, M., 2001, *Int.J.Mod.Phys.*, **D10**, 649-662
- Nowakowski, M., Sanabria, J. C. and García, A., 2002, *Phys.Rev.* **D66**, 023003
- Núñez, D., Matos, T. and Sussman, R. A., 2003, work in progress.
- Padmanabhan, T., 1990, *Physics Reports*, **188**, Number 5
- Structure formation in the universe*, Padmanabhan, T., 1995, Cambridge University Press
- Statistical Mechanics*, Pathria, R. K., 1972, Pergamon Press
- Quast, R. and Helbig, P., 1999, *Astron.Astrophys.*, textbf344, 721-744
- Salucci, P., Burkert, A., 2000, *ApJ*, 537, L9
- Shapiro, P. R. and Iliev, I. T., 2002, *ApJ*, 565, L1.
- Wang, L. and Steinhardt, P. J., 1998, *Ap J*, **508**, 483
- White, S. D. M., Rees, M. J., 1978, *MNRAS*, 183, 341
- Wilkinson, M. I., Kleyna, J., Evans, N. W., Gilmore, G., 2002, *MNRAS*, 330, 778
- Zehavi, I. and Dekel, A., 1999, *Nature*, **401**, 252,